



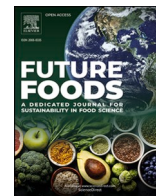
## Rheological behaviour of pea hull fibres treated with pectate lyase

Downloaded from: <https://research.chalmers.se>, 2026-04-16 04:24 UTC

Citation for the original published paper (version of record):

Ytterberg, J., Krona, A., Pereira, P. et al (2026). Rheological behaviour of pea hull fibres treated with pectate lyase. *Future Foods*, 13. <http://dx.doi.org/10.1016/j.fufo.2026.100945>

N.B. When citing this work, cite the original published paper.



## Rheological behaviour of pea hull fibres treated with pectate lyase

Jakob Ytterberg<sup>a</sup>, Annika Krona<sup>b</sup>, Pamela Freire de Moura Pereira<sup>c</sup>, Amparo Jimenez-Quero<sup>c</sup>, Patricia Lopez-Sanchez<sup>d,1</sup>, Anna Ström<sup>a,1</sup>

<sup>a</sup> Applied Chemistry, Department of Chemistry and Chemical Engineering, Chalmers University of Technology, Gothenburg, Sweden

<sup>b</sup> RISE Research Institutes of Sweden, Agriculture and Food, Box 5401, Gothenburg, Sweden

<sup>c</sup> Division of Industrial Biotechnology, Department of Life Sciences, Chalmers University of Technology, Gothenburg, Sweden

<sup>d</sup> Food Technology Department, Institute of Marine Research, Spanish National Research Council (IIM-CSIC), 36208 Vigo, Spain

### ARTICLE INFO

#### Keywords:

Pectate lyase  
Physicochemical properties  
Food technology  
Suspension  
Modelling particle rheology

### ABSTRACT

Side streams rich in irregular and deformable plant particles represent an untapped resource for sustainable food innovation. Pea hull fibres are an example of such underutilized, but increasing side stream material, whose functional limitation require targeted modification. In this study, we present a combined strategy using mechanical shearing and pectate lyase enzymatic treatment to enhance the functionality of pea hull fibres. This dual treatment alters their physicochemical properties, leading up to increase in their water retention capacity (WRC) and a shift in composition and microstructure revealed by optical microscopy. Enzymatic degradation of pectin improved water absorption and swelling ability, which translated into an increase in the viscosity of pea hull fibre suspensions. Importantly, we explore the rheological behaviour across an extended pea hull concentration range and identify three distinct regimes (dilute, intermediate and concentrated). These transitions were successfully captured and predicted using soft particle rheological models, demonstrating for the first time, the applicability of the models on suspensions based on pea hull fibres, as well as a prediction framework for pea hull fibre suspensions. Our findings show that mathematical models developed for soft plant particles can be used to predict suspension behaviour of pea hull fibres and establish a scalable approach to valorise plant-based side streams into high-performance functional ingredients.

### 1. Introduction

Plant material suspensions are encountered across sectors such as food, forestry and biofuels. In the food industry in particular, side streams generated during the extraction of protein or carbohydrates often consist of aqueous suspensions rich in irregular, polydisperse plant particles. These suspensions vary widely in particle size, shape and deformability, posing substantial challenges for both their characterization and functional exploitation. From a rheological perspective, most classical models are based on hard spheres as particles (Mewis & Wagner, 2009), which do not adequately reflect the nature of food suspensions, systems that are largely dominated by soft matter compounds such as swollen plant cells and droplets (Mezzenga et al., 2005). This soft and deformable nature becomes especially critical at higher particle concentrations, where interactions become increasingly elastic and complex, influencing both behaviour and texture. In food applications, where texture, hydration, and processability are key, lack of understanding the structure-rheology relationship constrains the

valorisation of these streams into functional ingredients.

In case of soft particle suspensions, the concentration dependence becomes complex, often exhibiting viscoelastic properties at high concentration under low shear conditions (Lopez-Sanchez & Farr, 2012; Shewan & Stokes, 2015). Above a certain yield stress, the suspension starts to flow. Both experimental studies and computer simulations have attempted to develop unified models to describe the behaviour of soft particle suspension, going beyond existing models designed for rigid particles. The earliest model describing suspension rheology was proposed by Einstein for hard spheres in dilute conditions. The Einstein model was later modified by Krieger-Dougherty and Quemada including the semi-dilute regime (Krieger & Dougherty, 1959; Quemada, 1977). However, Einstein and Krieger-Dougherty and Quemada models fall short when applied to consider the deformation in particle morphology that happens at higher concentrations of soft particles (Leverrier et al., 2021).

Studies on soft particles suspensions in industrial food applications systems, has been conducted using broccoli, carrot and tomato as

<sup>1</sup> Joint corresponding author.

resources (Bayod et al., 2007; Day, Xu et al., 2010; Lopez-Sanchez et al., 2012; Lopez-Sanchez & Farr, 2012). These studies focus on specific concentration regions and did not show a unified model over a wide concentration range to predict suspension properties. On the other hand, Leverrier and colleagues demonstrated that the rheological properties of apple purees align that of models for soft particle suspensions. Expanding on a model by Mendoza, Leverrier and colleagues showed that the flow behaviour of apple purees could be predicted/modelled across different concentration regimes (Leverrier et al., 2021; Leverrier et al., 2016; Mendoza, 2013).

Pea hulls are a side stream generated during the processing of yellow peas (*Pisum Sativum L.*) or extraction of protein from yellow peas (*Pisum Sativum L.*). Pea hull fibres have limited uses in the food industry owing to poor techno-functional properties. Currently, pea hull fibres are mainly used to enrich fibre content of food products (Ratnayake & Naguleswaran, 2022). Improved functionality, and uses of the pea hull fibres can reduce waste in the food system and increase circularity. Pea hull fibres have interesting nutritional properties in terms of high fibre content and low allergenicity (Auffret, Ralet, Guillon et al., 1994; Boukid, Rosell, & Castellari, 2021). The poor techno-functional properties of pea hull fibres relates to their large particle size, their insolubility in water and oil, as well as limited water retention capacity (Tosh & Yada, 2010). Methods, aimed at improving the functionality, have particularly targeted increased water retention, viscosity and viscoelasticity of pea hull fibre dispersions. These approaches include grinding (Auffret et al., 1994), heating (Karlsson et al., 2024), extrusion (Kumari, Das, & Deka, 2022), microfluidisation (Morales-Medina et al., 2020; Morales-Medina, Manthei, & Drusch, 2024), chemical extraction (Gutöhrlein et al., 2020; Ramirez, Temelli, & Saldaña, 2021) and enzymatic hydrolysis (Kumari et al., 2023; Morales-Medina et al., 2024). Among the enzymes tested, cellulases, hemicellulases (e.g., xylanase), and pectinases are the most commonly applied. Pectinases are a varied group of enzymes (e.g. polygalacturonases (PG), pectin methyl esterases (PME) and pectate lyases (PL)) with different active sites. So far, mixtures of PG, PME and PL has been tested on pea hull fibres, but not individual pectinases (Morales-Medina et al., 2024). Morales-Medina and colleagues demonstrated that a combined enzymatic pre-treatment improved the water-binding and rheological properties of pea hull fibre suspensions (Morales-Medina et al., 2024). Notably, the mixture of cellulase and hemicellulase combined with microfluidisation yielded the most significant change in water binding, viscosity and viscoelasticity. These improvements were attributed to the release of high molecular weight polysaccharides, which were absent in other enzymatic pre-treatments, probably due to the reduction of the interaction/crosslink between cellulose and pectins. Similarly, Kumari and colleagues showed that enzymatic treatment of green pea hulls using cellulase and xylanase enhanced swelling, water holding and surface area of the green pea hull fibre (Kumari et al., 2022).

In this study, we investigated the impact of mechanical shearing combined with enzymatic hydrolysis of pea hull fibres using PL. PL have importance in the softening of plants and fruits, and has multiple applications in pulping, food and textile industry (Uluisik & Seymour, 2020; Wu et al., 2020) but has of yet not been tested for functionalisation of pea hull fibre. To assess the effectiveness of the treatment, we characterized the composition, particle size distribution (PSD), Brunauer–Emmett–Teller (BET) surface area, particle microstructure and water retention capacity (WRC) of the resulting pea hull fibre. The suspension behaviour of the sheared and hydrolysed pea hull fibre was determined using flow and oscillatory rheological measurements across several concentration regimes. The rheological results were analysed using established models for soft particle suspensions, allowing us to contextualize the behaviour of the pea hull fibre within a broader framework of suspension systems.

## 2. Materials and methods

### 2.1. Materials

The yellow pea hull fibre was Vestkorn Fibradan® F20X (Vestkorn Milling A/S, Denmark) with 89.5 % total dietary fibres on a dry base as provided by the supplier. The dietary fibres mainly consist of glucose (62 %), xylose (15.5 %), uronic acids (13.6 %) and arabinose (5.6 %), with smaller fractions of other monosaccharides (Karlsson et al., 2024). Pectate lyase (*Aspergillus sp.*) (180 U/mg) were acquired from Megazyme Ltd, Bray, Ireland. All chemicals used were obtained from Merck (Darmstadt, Germany) unless otherwise stated and were of analytical grade.

### 2.2. Sample preparation and enzymatic hydrolysis

The different samples were prepared in multiple steps (Fig. 1). A total of three samples were prepared; untreated (U), sheared (S) and sheared and pectate lyase treatment (P). Untreated pea hull fibre samples (U, U-I and U-Sol) were prepared by adding 450ml of Milli-Q (MQ) water to 50g of pea hull fibres (10 % w/w). The dispersion was stirred at 20°C for one hour, centrifuged at 12,000 g for 10 minutes and then separated by pellet (called untreated-insoluble, or U-I) and supernatant (called untreated supernatant, or U-Sol). A non-centrifuged sample containing both insoluble and soluble fractions was called U. All samples were then freeze-dried for use in further analysis. From here on, “I” in the sample name stands for the insoluble part of the suspension (pellet) and “Sol” for the supernatant.

A mechanically sheared sample (S, S-I and S-Sol) was prepared in the same way as U but with the added step of mechanical shearing. To shear the suspension, a Silverson L5M-A (Chesham, UK) was used at 7,000 rpm for two minutes. Centrifugation, separation and freeze-drying followed in the same way as with the U samples.

The enzymatically hydrolysed sample with pectate lyase (P, P-I and P-Sol) was prepared by adding a buffer of 450ml of pH 8, 100mM phosphate buffered saline (PBS) to 10g of pea hull fibres. The Silverson L5M-A (7,000 rpm for two minutes) was then used for mechanical shearing. The dispersion was heated to 45°C under stirring and pectate lyase (5 U/g pea hull fibre) was added and allowed to react for 24 hours. To stop the hydrolysis, the temperature was increased to 90°C for 10 minutes. The final steps of centrifugation, separation and freeze-drying were performed as with the U samples.

### 2.3. Monosaccharide analysis

The neutral monosaccharide content of the pea hull fibre samples were determined using a modified method described by Sluiter and coauthors (Sluiter et al., 2008). Shortly, 200mg of sample was added to a 150ml beaker, and mixed with 3ml 72 % H<sub>2</sub>SO<sub>4</sub>. The beaker was placed under vacuum for 15 minutes and then immersed in a water bath at 30°C for one hour. Every 20 minutes, the samples were stirred and 84g deionised water was added after the one hour. Samples were autoclaved at 125°C for one hour and then filtered through vacuum. All samples were then diluted to 100 ml and fucose was added as an internal standard at 400mg fucose/L. Samples were filtered into HPLC vials through 0.45µm syringe filters.

The analysis was performed using high-performance anion exchange chromatography (HPAEC) with a pulsed amperometry detector (PAD) (ICS 3000 Dionex, Sunnyvale, USA). The system was equipped with an AEC column CarboPac PA 1 analytical (4 × 250mm) and Milli-Q water was used as mobile phase. Cleaning using 60 % v/v 200mM NaOH and 40 % v/v 200mM NaOH +170mM NaOAc was injected between the samples. The flow was 0.13ml/min and post column 200mM NaOH was added. D (+) glucose, D (+) xylose, D (+) galactose, L (+) arabinose, L (+) rhamnose and D (+) mannose was used as standards.

Uronic acids (galacturonic acid and glucuronic acid) was analysed

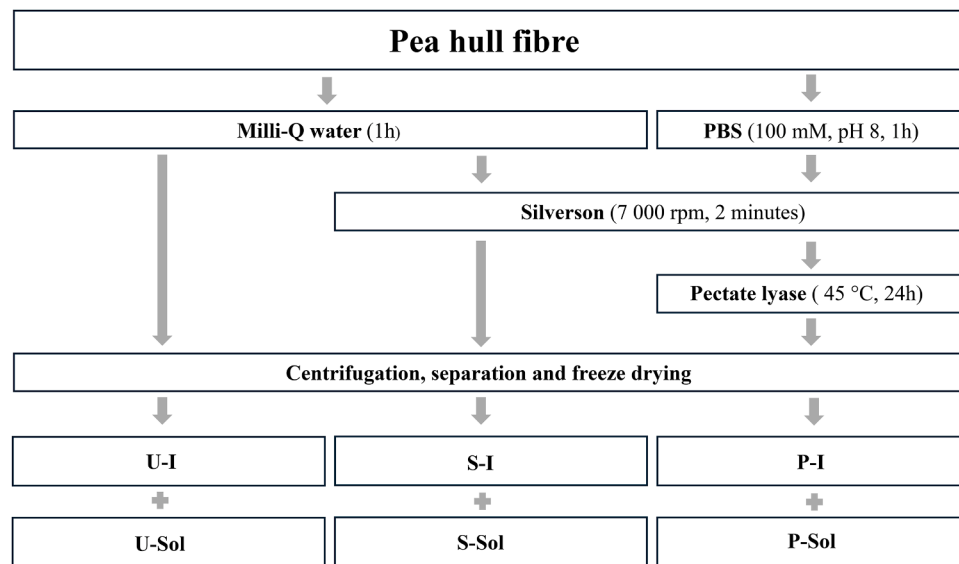


**Fig. 1.** Overview of the sample preparation for the four different pathways, with eight samples in total. The pathways are untreated pea hull fibre (U), mechanically sheared pea hull fibre (S) and enzymatic hydrolysis of pea hull fibre with pectate lyase (P). The I and Sol denote the insoluble and solubilised fractions after centrifugation.

according to Massironi and coauthors (Massironi et al., 2024). There, the samples were subjected to a two-step methanolysis followed by trifluoroacetic acid (TFA) hydrolysis. The quantities were determined in a high-performance anion exchange chromatography coupled with a pulsed amperometric detection (HPAEC-PAD) (ICS-6000 Dionex, Thermo Fischer, USA). The column used was a CarboPac™ PA20 (3 × 150mm) at a flow of 0.4ml/min. A gradient method was employed using Milli-Q water, 200 mM NaOH, and 100 mM NaOH +100 mM NaAc, as eluents A, B, and C. The method was as following: 1.2 % of B for 8min of equilibration; 1.2 % B for 20min; 50 % B for 10.1min; 100 % C for 15.9min; 100 % B for 3.9min; 1.2 % B for 10.1min. Galacturonic acid and glucuronic acid was used as standards.

#### 2.4. Particle size analysis

To measure the particle size distribution (PSD), 1 % (w/w) suspensions of the samples were prepared. Then, 0.5ml of suspension was added dropwise to a Mastersizer 2000 (Malvern Instruments Ltd, Malvern, UK) equipped with a 2000 Hydro-SM accessory, filled with 100ml of deionised water. A refractive index of 1.47, absorption of 0.01 and obscuration range 5-10 % was used. A model for irregular shape was selected due to the anisotropic shape of the particle. The volume-based  $D_{[4,3]}$  and surface area-based  $D_{[3,2]}$  average diameters (Equations 1 and 2) were calculated from the intensity profiles of the scattered light using the instrument software (Mastersizer 2000, version 6.01).

$$D_{[4,3]} = \frac{\sum_i n_i d_i^4}{\sum_i n_i d_i^3} \quad (1)$$

$$D_{[3,2]} = \frac{\sum_i n_i d_i^3}{\sum_i n_i d_i^2} \quad (2)$$

In Eq. 1 and Eq. 2,  $n_i$  is the number of particles and  $d_i$  is the diameter of the particle.

#### 2.5. Water retention capacity (WRC)

The WRC of the pea hull fibres was measured according to Johansson and colleagues (Johansson et al., 2024). Suspensions at 5 % (w/w) in distilled water were prepared for each sample. The suspensions were left agitating overnight on a PSU-20i Orbital Shaking Platform (Grant

Instruments, Cambridge, UK) and then centrifuged at 580 x g for 10 minutes. Excess water was removed using a pipette and the remaining sample was weighted. The WRC was calculated as grams of retained water per gram of dry sample.

#### 2.6. Brunauer-Emmet-Teller (BET) surface area

The BET surface area of the pea hull fibres was determined using a Tristar 3000 (Micromeritics Instrument Corporation, Norcross, US). The samples were degassed at 60°C under vacuum ( $P = 2\mu\text{mHg}$ ) with an ASAP 2020 PLUS (Micromeritics Instrument Corporation, Norcross, US). Nitrogen at -196°C was used as adsorption gas with the relative pressure ( $P/P_0$ ) ranging from 0.01 to 0.98 for the adsorption isotherm. The BET surface area was calculated according to the consistency criteria (Rouquerol et al., 2007).

#### 2.7. X-ray diffraction (XRD) analysis

Diffractionograms with X-rays of pea hull fibres were obtained using a diffractometer (D8 Discover, Bruker, Berlin, Germany). The radiation source was a Cu K $\alpha$  ( $\lambda = 1.54\text{\AA}$ ), covering  $2\theta$  from 5° - 60°. The exposure duration and total analysis time for each sample was 2,100 seconds. The pea hull fibre powder was mounted on single crystal Si holders. A qualitative comparison of the crystallinity index in the samples was performed using the Segal peak height method according to Segal, Creely, Martin Jr, and Conrad (1959) (Segal et al., 1959).

#### 2.8. Microstructural characterisation using light microscopy

Samples were frozen in liquid nitrogen and mounted to holders before being cryo-sectioned into 8 $\mu\text{m}$  thick sections in a Leica CM3050S cryostat. The sections were then applied to Polysine® microscope slides (VWR International, Radnor, USA). Hydrated sections were examined via an Olympus BX53 light microscope (Olympus Life Science, Tokyo, Japan) with a 20x objective, using differential interference contrast (DIC) imaging to increase the contrast of different structures. At least 10 micrographs were captured for each sample with a CMOS SC50 camera (Olympus Life Science) and processed using the Olympus cellSense Entry software.

2.9. Flow and oscillatory analysis

The rheological measurements were carried out using a rheometer DHR-3 (TA Instruments, New Castle, USA). The geometry equipment used depended on the sample being measured. A 40mm parallel plate geometry was used for pellet samples (U-I, S-I and P-I).

Flow measurements using the parallel plate geometry used a gap of 1mm, while the cone-and-plate geometry used a 57µm truncation gap. A Peltier plate was used to maintain the temperature at 25°C. MQ water was added to the freeze-dried samples and stirred overnight in a closed vial. The samples were added to the rheometer using a pipette and pre-sheared at 10 s<sup>-1</sup> for 10 seconds and then rested for one minute, followed by shear sweep between 0.01 s<sup>-1</sup> and 100 s<sup>-1</sup>. The displayed viscosity measurements are shown as η<sub>relative</sub> and are calculated as Eq. 3.

$$\eta_{relative} = \frac{\eta_{measured}}{\eta_0} \tag{3}$$

where η<sub>measured</sub> is the measured absolute viscosity and η<sub>0</sub> is the viscosity of the suspension liquid.

Oscillatory measurements used a 1mm gap and a 57µm truncation gap for the parallel plate and cone-and-plate geometries respectively. A Peltier plate was used to maintain the temperature at 25°C. Samples were stirred overnight with MQ-water in closed vials before measurement. The samples were pipetted and loaded into the rheometer and pre-sheared at 10 s<sup>-1</sup> for 10 s and then rested for one minute. The strain (γ) sweep ranged from 0.01 to 100 %, with a frequency of 6.28 rad/s. Datapoints for the G' and G'' were taken within the linear viscoelastic region (LVR).

2.10. Particle suspension models

The rheological measurements for the P-I sample were fitted to existing particle suspension models, (Table 1). All analysis and model-fitting were conducted in OriginPro 2023 version 10.0.0.154 (OriginLab).

2.11. Statistical analysis

Fractions of the soluble and insoluble pea hull fibre, WRC, particle size and BET surface area were measured in triplicate. Statistical significance was calculated using analysis of variance (ANOVA) with a significant level of 5 %. When ANOVA results were significant, a Tukey's post-hoc test was used to compare group means. The statistical analysis was done using Python in Visual Studio Code (version 1.99.3). All rheological measurements were done in triplicate.

Table 2

Total monosaccharides in the hydrolysed samples stated in g/100 g sample.

Sample	U-I	U-S	S-I	S-S	P-I	P-S
Arabinose	3.4	5.1	3.3	7.2	2.8	4.5
Rhamnose	0.2	0.6	0.2	0.5	0.2	0.5
Galactose	1.1	3.6	1.1	4.8	0.8	1.9
Glucose	35.5	3.9	33.8	2.6	36.0	n.d
Xylose	13.3	9.3	13.0	10.3	13.6	3.7
Mannose	0.2	0.1	0.1	n.d	0.1	n.d
Galacturonic acid*	6.4	7.2	8.7	6.9	5.8	10.8
Glucuronic acid*	3.6	1.2	5.4	1.5	3.9	6.9
Total	63.7	31.0	65.6	33.8	63.2	28.3

n.d – monosaccharide content below limit of detection (<1mg/L)

\*Galacturonic acid and glucuronic acid content was determined using meth-analysis (Massironi et al., 2024).

3. Results and discussion

3.1. Impact of enzymatic hydrolysis on particle composition and properties

The monosaccharide composition of the insoluble fractions (U-I, S-I and P-I) were primarily composed by glucose, xylose, and galacturonic acid (GalA), reflecting the presence of cellulose, hemicellulose and pectin in the pea hull fibre (Table 2) (Karlsson et al., 2024; Ralet et al., 1993). No or minor difference of the insoluble part was obtained between treatments. In contrast, the soluble fractions (U-S, S-S and P-S) displayed more pronounced differences. Notably, U-S and S-S containing higher amounts of xylose, GalA and arabinose, while glucose remained low in all soluble fractions, suggesting that cellulose remains in the insoluble fraction after mechanical shearing. The P-S sample had the largest concentration of GalA (10.8 g/100g) and glucuronic acid (GlcA) (6.9 g/100g), which indicates that pectate lyase can access and degrade the pectin, resulting in enhanced pectin solubilisation. These findings confirm the selective degradation of pectic polysaccharides, validating the enzyme's efficiency in targeting pectin components within the fibre matrix. However, the persistence of a notable pectin fraction in the P-I sample suggests that part of the pectin was inaccessible by pectate lyase, and that further hydrolysis might enhance other physicochemical properties more markedly.

Among the solubilised fractions, no significant differences (p = 0.07) in total mass were observed between the treatments. However, it is possible to note the solubilisation trend to be higher for P treated samples (8.0 %), in comparison with U (5.1 %) and S (5.4 %) samples (Table 3). The trend of increased mass solubilised mirrors the changed observed in water retention capacity (WRC). The untreated sample

Table 1

All models used for fitting the flow and oscillatory data. Equations 4 to 7 are used to fit specific concentration regimes (dilute, intermediate and concentrated). Equations 8 to 10 are used to fit the entire concentration range.

$\eta(c) = \eta_0(1 + kc)$	eq. 4	(Einstein, 1906)
$\eta(c) = ac^b$	eq. 5	(Leverrier, Almeida, Menut, & Cuvelier, 2017)
$\eta(c) = \eta_0(a + b \ln c)$	eq. 6	(Leverrier et al., 2017)
$G' = A \left(1 - \frac{\phi_c}{\phi}\right)^{\frac{1}{3}}$	eq. 7	(Adams, Frith, & Stokes, 2004)
$\eta(\phi) = \eta_0 \left(1 - \frac{\phi}{\phi_{rcp}}\right)^{-k\phi_{rcp}}$	eq. 8	(Krieger & Dougherty, 1959)
$\eta(\phi) = \eta_0 \left(1 - \frac{\phi}{1 - k\phi}\right)^{- \eta }$ ; $k = \frac{1 - \phi_c}{\phi_c}$ ; $\phi_c = \phi_{rcp} + \beta\phi^a$	eq. 9	(Mendoza, 2013)
$\eta(\phi) = \eta_0 \left(1 - \frac{\phi}{1 - k\phi}\right)^{-S}$ ; $k = \frac{1 - \phi_c}{\phi_c}$ ; $\phi_c = \phi_{rcp} + \frac{\phi_{max} - \phi_{rcp}}{1 + \exp[-\Lambda(\phi - \phi_1)]}$	eq. 10	(Leverrier et al., 2021)

Note: For eq. 4, 5 and 6, η(c) is the viscosity, η<sub>0</sub> is the viscosity of the suspension liquid and c is the concentration of the particles in g/100g. k, a and b are coefficients. For eq.7, G' is the storage modulus, φ<sub>c</sub> is the critical volume fraction, φ is the volume fraction and A is a coefficient. For eq. 8, 9 and 10, η(φ) is the viscosity, η<sub>0</sub> is the viscosity of the suspension liquid, φ is the volume fraction, φ<sub>rcp</sub> is the volume fraction at random close packing. k, [η], β, α, S, φ<sub>max</sub>, φ<sub>1</sub> and Λ are coefficients.

**Table 3**

The insoluble fraction (I), solubilised fraction (Sol), WRC, particle size ( $D_{[4,3]}$ ), BET surface area and crystallinity index of samples prepared with three different preparation methods.

Sample	I fraction (wt %)	Sol fraction (wt %)	WRC (ml/g)	$D_{[4,3]}$ ( $\mu\text{m}$ )	BET surface area ( $\text{m}^2/\text{g}$ )	Crystallinity index (%)
Untreated (U)	94.9 $\pm$ 1.5 <sup>a</sup>	5.1 $\pm$ 1.5 <sup>a</sup>	5.1 $\pm$ 0.1 <sup>a</sup>	338.5 $\pm$ 3.4 <sup>a</sup>	0.53 $\pm$ 0.01 <sup>a</sup>	61.4
Sheared (S)	94.6 $\pm$ 1.6 <sup>a</sup>	5.4 $\pm$ 1.6 <sup>a</sup>	5.7 $\pm$ 0.2 <sup>b</sup>	358.6 $\pm$ 6.0 <sup>b</sup>	0.56 $\pm$ 0.16 <sup>a</sup>	63.0
Sheared and pectate lyase (P)	92.0 $\pm$ 0.7 <sup>a</sup>	8.0 $\pm$ 0.7 <sup>a</sup>	5.9 $\pm$ 0.2 <sup>b</sup>	368.0 $\pm$ 11.1 <sup>b</sup>	0.66 $\pm$ 0.10 <sup>a</sup>	61.7

The values are expressed in mean  $\pm$  standard with  $n = 3$ . The different letters in superscript indicate values that are significantly different at  $p < 0.05$ . Means values not expressed with letters represent samples with no statistical significance by ANOVA assay.

showed the lowest WRC (5.1ml/g), which was statistically significantly lower than the WRC of both S and P samples, ranging from 5.7 to 5.9, respectively. The values of WRC obtained here were similar to those obtained using chemical treatment (Gutöhrlein et al., 2020) but lower than the WRC observed by Morales-Medina and colleagues. The comparison indicate that the micro-fluidisation step in the study done by Morales-Medina and colleagues, is a major contributor for increasing the WRC of pea hull fibres (Morales-Medina et al., 2024).

The volume weighted mean diameter ( $D_{[4,3]}$ ) of the particles varied on response to the treatment. Interestingly, the size for the untreated fibre (338.5 $\mu\text{m}$ ) was statistically significantly smaller ( $p = 0.008$ ) than the S and P samples. The apparent increase in  $D_{[4,3]}$  after shearing and enzymatic hydrolysis is most probably due to increased swelling of the particles after treatment. Degradation of the pectin in the fibre particles result in a more porous structure and thus a higher water uptake and swelling (Morales-Medina et al., 2024). An increase in porous structure is supported by the increase in WRC of the enzymatically treated pea hull fibres, but not by the surface area as determined using BET. The lack of statistically significant variation in BET, is in contrast to results obtained by Kumari and colleagues, where an increased BET surface area was shown after enzymatic modification with cellulase and xylanase on the peel of green pea (Kumari et al., 2022). The particle size distribution (PSD) of the insoluble fraction for the different preparation methods shifted slightly after pectate lyase treatment (Fig. 2). The crystallinity index measured with XRD was not affected by shearing or enzymatic hydrolysis. Crystalline parts of the pea hull fibre are expected to be cellulose, which are unaffected by the shear or PL hydrolysis (degradation of pectin).

The P-I sample shows a larger proportion of small ( $< 100\mu\text{m}$ ) and large ( $> 1000\mu\text{m}$ ) particles. The smaller fraction at  $< 100\mu\text{m}$  is likely caused by pea hull fibre degradation by the pectate lyase, while the fraction that is  $> 1000\mu\text{m}$  can be explained by the PL producing a more porous structure pea hull fibre and thereby increasing its water uptake. In contrast, the PSD of the S-I sample remained similar to the untreated U-I sample, indicating that mechanical shearing alone had a limited impact on fibre breakdown and porosity.

The microstructure of the pea hull fibre is visible using light microscopy (Fig. 3). There is a noticeable difference between the U-I and the P-I sample. After the use of mechanical shearing and PL hydrolysis, the cell structure showed a more disrupted and irregular morphology, as compared to the starting material. The combined effect of mechanical shearing and pectate lyase hydrolysis caused the cell structure to collapse, reducing structural uniformity. These observation are consistent with the role of pectin supporting the cell structure and contributing to the loadbearing properties, where pectin degradation drives to a less rigid structure (Broxterman & Schols, 2018; Höfte et al., 2012).

### 3.2. Comparison of the rheological behaviour of suspensions

In order to understand the macroscopic or suspension behaviour of the pea hull fibre, the reconstituted insoluble fractions of the untreated, sheared and sheared and PL treated pea hull fibre was studied. The P-I sample has a higher viscosity at 6g and 12g/100g  $\text{H}_2\text{O}$  (Fig. 4). The change in viscosity of P-I compared to U-I aligns with the changes observed using WRC and microscopy, with the explanation of increased swelling and water uptake being enabled through a less rigid plant cell

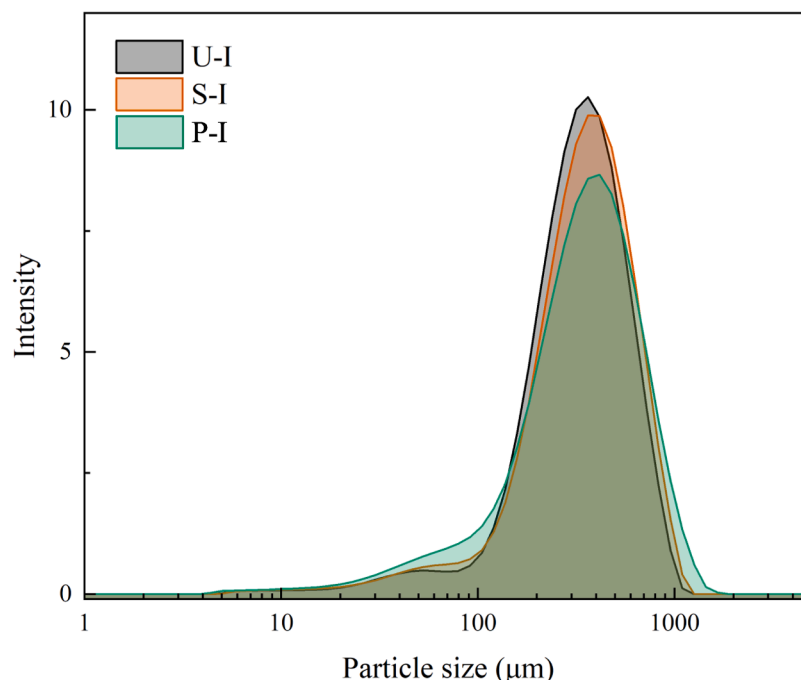


**Fig. 2.** Particle size distribution (PSD) of the U-I (black), S-I (orange), P-I (green).

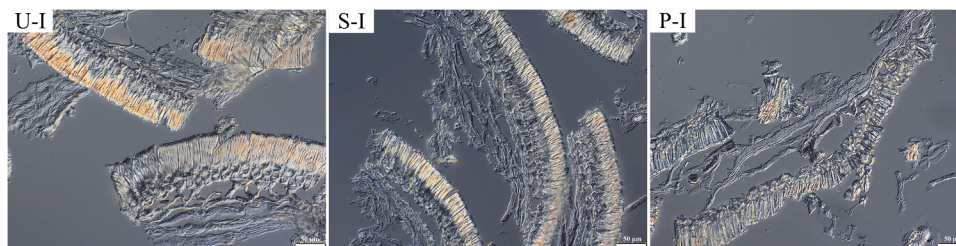


**Fig. 3.** Light microscopy images of pea hull fibre after different treatments. The untreated insoluble fraction (U-I), sheared insoluble fraction (S-I) and sheared and pectinase insoluble fraction (P-I) are the samples shown. Scalebar: 50µm.

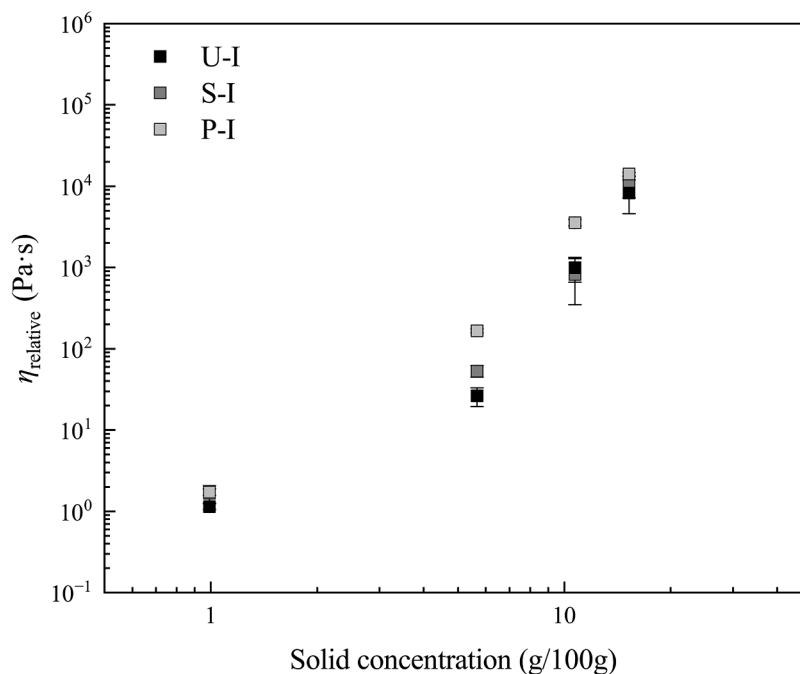


**Fig. 4.** Flow sweep measurements of the reconstituted insoluble fraction in water. The reconstituted insoluble fraction was measured at four concentrations (1, 6, 12 and 18g/100g H<sub>2</sub>O). The samples were U-I (black), S-I (dark grey) and P-I (light grey).

wall structure. The P-I sample is expected to occupy a larger volume fraction at the same solid concentration and thus has a higher relative viscosity.

Additionally, the  $\eta_{\text{relative}}$  of the reconstituted insoluble fraction in water (U-I, S-I and P-I) and that of the full samples was compared (not shown). The viscosity is similar, suggesting that the viscosity of all samples is dominated by the insoluble particles. There is no obvious trend when observing the full samples at different concentrations, regardless of the sample preparation; the variation could be due to the limited control of the serum phase for the full sample.

### 3.3. Modelling of the rheological properties: hard vs soft particle behaviour

Additional flow sweep measurements were performed on the reconstituted P-I sample, in order to study the suspension behaviour in a broader concentration regime. The particle concentration was widened to range from 0.1g/100g to 18.7g/100g. Three regimes were observed in this concentration span and named I, II and III (Fig. 5). These three regimes have been observed in plant cell wall suspensions and fitted individually using particle models (Leverrier et al., 2016).

Below 2.3g/100g the suspension is in the first regime (I), where the viscosity is not dependent on particle properties. As seen in Fig. 5, the viscosity of the samples has no or little dependence on solid

concentration in this regime. The suspensions exhibited Newtonian behaviour and can be fitted to Einstein's linear model, see Eq. 4 (Table 1). In this model, the volume fraction of hard spheres relative to the suspension viscosity generates a slope of  $k = 2.5$ . A value greater than 2.5 would indicate stronger hydrodynamic interaction between the particles, while a lower value suggests weak interactions. The P-I sample displays a lower slope in the dilute region, around 0.3, which indicate neither aggregation nor particle interaction occurring under shear (Supplementary Fig. S.1 and Table S.1) (Leverrier et al., 2016). At this concentration, sedimentation occurs, which is why the viscosity is close to that of the liquid phase (water).

The viscosity increases rapidly in the second regime (II), to between 2.3g/100g and 11.6g/100g. The viscosity results can be modelled using a power law equation (Equation 5, Table 1), similar to what has been used for carrot suspensions (Lopez-Sanchez et al., 2012; Lopez-Sanchez & Farr, 2012), where  $c$  is the concentration of insoluble particles (Supplementary Fig. S.1 and Table S.1). A  $b$  value of 4.7 was observed, which is higher than the observed value of  $\sim 2$  for apple purees (Leverrier et al., 2016). The absolute value of  $b$  increases with the particle polydispersity, which agrees well with the large PSD we observed for P-I (Fig. 1). The sharp increase in viscosity is due to particle-particle interactions. The main interactions between the particles are long-range hydrodynamic interactions but the viscous deformation is also influenced by lubrication forces and friction between the particles when sliding past each

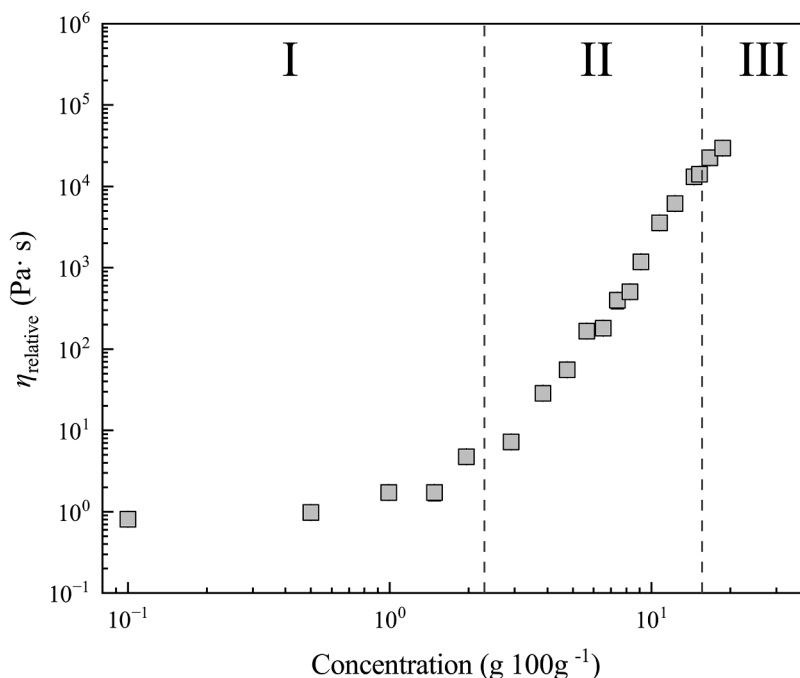


**Fig. 5.** Viscosity as a function of total solid content for the P-I sample ranging from 0.1 to 18.7g/100g. The three concentration regimes visualised are the dilute (I), intermediate (II) and concentrated (III) domains.

other (Lopez-Sanchez et al., 2012).

The third regime (III) is reached when the insoluble solid concentration reaches 11.6g/100g. The viscosity in the third regime is less dependent on particle size and shape, as the particles are closely packed and, in the case of soft particles, they can deform to fit into the available space. However, the concentration at which the suspension enters this regime depends on the particle properties. A greater polydispersity and particle size allow the system to reach a concentrated state, or regime III at lower particle content (Servais, Jones, & Roberts, 2002). The presence

of small particles allows them to fit into the voids between larger particles and, therefore, pack efficiently at lower concentrations. Thus, a higher concentration would be required to reach the same viscosity as a monodisperse sample. A logarithmic approach was used to fit this region using models inspired by the compaction in clay and cement-based materials (Eq. 6, Table 1) (Khelifi et al., 2013; Leverrier et al., 2016). The logarithmic function is used to fit the disappearance of available space between the particles, which can also be applied to our case (Supplementary Fig. S.1 and Table S.1).

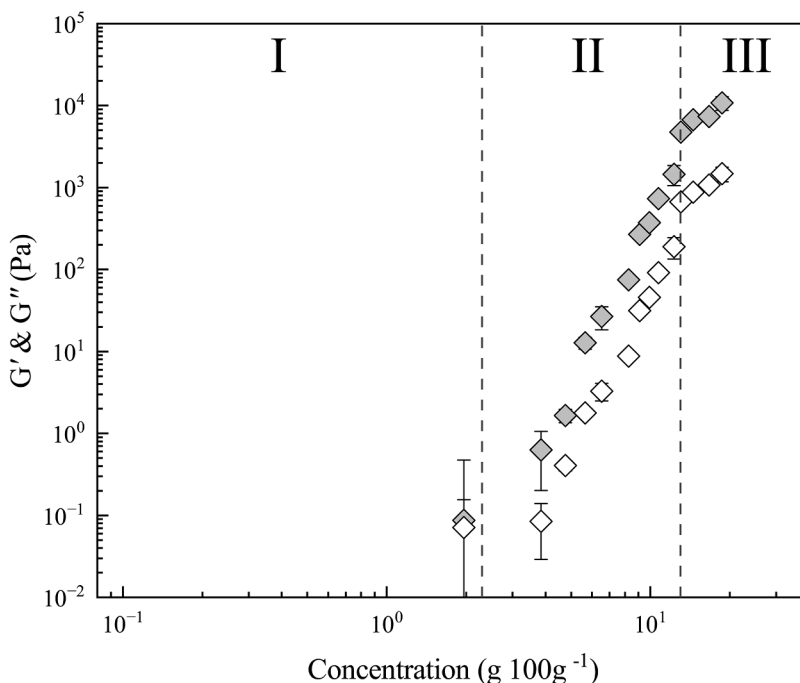


**Fig. 6.** Storage (grey) and loss (white) modulus of the P-I sample in the concentration range of 2.0 to 18.7g/100g H<sub>2</sub>O. The concentration regimes visualised are the same as in Fig. 5; dilute (I), intermediate (II) and concentrated (III).

Viscoelastic properties of the P-I suspension were evaluated in similar fashion to the viscous properties (Fig. 6). The three regimes (dilute, intermediate, concentrated) are also observed for oscillatory measurements ( $G'$ ) as a function of concentration. However, the shift between regimes I and II is less clear. Regimes I and II can be modelled using the functions previously used for the viscosity measurements, as the dilute and intermediate regions display identical behaviour, (Supplementary Fig. S.2 and Table S.1). However, given the absence of percolating particle network formation, oscillatory measurements at low total solid content (< 2g/100g) yielded no meaningful data. The regime shift (I to II) was therefore set to the same concentration as predicted in the viscosity data. Leverrier and co-authors encountered a similar problem when investigating apple puree but observed that the regime shift predicted by the viscosity and viscoelastic data agreed (Leverrier et al., 2016). The second regime was fitted with a power-law equation and has the exponent value of  $b = 8.1$ , which is significantly higher than the value observed in the viscosity data and by Leverrier. Leverrier and colleagues observed an increasing exponent value with increasing particle size and irregular shape. P-I has large particle size, PSD and non-spherical shape which would indicate a large  $b$  value. The large particle size causes the particle to jam at lower concentrations and thus generate a network. Smaller particles within a polydisperse sample can fill the void space between the larger particles, enhancing the rigidity of the network (Farr & Groot, 2009; Farris, 1968).

At high concentration, the third regime is reached (III), where the  $G' \gg G''$ . This region can be modelled using an equation proposed by Adams and co-authors (Equation 7, Table 1) (Adams et al., 2004). The equation uses the volume fraction  $\phi$ , critical volume fraction  $\phi_c$  (where the particles are closely packed) and a variable constant  $A$ . To use this model, a simplification was made, with the total insoluble particle concentration ( $c$  and  $c_c$ ) used instead of the volume fraction. The critical packing concentration ( $c_c$ ) was predicted at 10.8g/100g using the Adams model, which is close to the observed value of 11.6g/100g for the viscosity measurements.

The separate regimes in the viscosity and viscoelastic measurements have previously been modelled. However, when it comes to a unified model for the entire concentration range, complexity increases. One problem is that most models (such as Einstein, Krieger-Dougherty and Mendoza) use the volume fraction occupied by the insoluble particles, rather than the total insoluble particle concentration. This brings complications because there are limited methods of determining the volume fraction for soft particles (Boehm, Warren, Baier, Gidley, & Stokes, 2019). The challenge when it comes to predicting suspension behaviour is to determine the *de facto* volume fraction that the particles occupy. Centrifugation or sedimentation is common and simple ways to measure the volume fraction but, in the case of soft particles, the volume occupied by those particles will change when force is applied during centrifugation (Boehm et al., 2019; Poon, Weeks, & Royall, 2012). This will result in a volume fraction depending on the force applied during centrifugation and is thus not representative of the volume fraction in the initial suspension/sample (Lopez-Sanchez et al., 2012). A way around this problem is to use a theoretical approach to calculate the volume fraction instead, similar to what was shown earlier by Day and colleagues (Day et al., 2010) and Leverrier and colleagues (Leverrier et al., 2016). Plant cell particles can pack with greater efficiency compared to hard spheres, which only reaches a maximum volume fraction of 74 %. The plant cells can deform and will therefore fit into the shrinking available space, even at high particle concentrations. Thus, the concentration at which the regime shifts between II and III (now noted as  $c^{**}$ ) can be assumed to be equal to a volume fraction of 1. Subsequently,  $c^{**}$  is thereby defined as the concentration at which the particles occupy all the volume but do not deform or shrink. This methodology works for viscosity measurements (Leverrier et al., 2016) and viscoelastic measurements (Day et al., 2010). For our measurements, the  $c^{**}$  of the P-I sample occurs at 15.6g/100g for the viscous data and 13g/100g for the viscoelastic data. Thus, the exact

concentration at which  $c^{**}$  is obtained differs between the two rheological properties. The total insoluble particle concentration can be converted to an apparent volume fraction by using  $c^{**}$  from the viscous data, see Eq. 11.

$$\phi_{app} = \frac{c}{c^{**}} \quad (11)$$

With an apparent volume fraction defined, it is possible to use established models to predict the rheological behaviour (Table 1). A simple model to fit the dilute region could be the Einstein model (Eq. 4, Table 1). As this model only examines dispersions with no particle interactions (thus exhibiting only Newtonian behaviour) it would not be a good fit for the whole concentration range. A natural step towards expanding the Einstein model is to introduce a parameter to limit the maximum packing density. This was done by Krieger and Dougherty who modelled hard spheres, giving a maximum packing of 0.635 due to random close packing (Table 4 and Fig. 7) (Krieger & Dougherty, 1959). The Krieger-Dougherty model introduces behaviour for non-Newtonian suspensions and more accurately fits our data in the intermediate region but is limited by the maximum packing density. The model covers a greater proportion of the concentration regimes compared to the Einstein model and generates a  $k$  value of 3.9, which is closer to the theoretical value for hard-sphere systems. The limitation of the Krieger-Dougherty model is that it does not consider particle shape or deformability. This causes it to deviate from the complexity of the P-I sample.

A follow-up was proposed by Mendoza to introduce a variable critical packing parameter, which allows the maximum packing efficiency to extend above random close packing, whilst including hydrodynamic interactions and crowding effects (Table 4) (Mendoza, 2013). This model fits the data well in the entire volume fraction range. The  $[\eta]$  value is comparable to the  $k$  value for the previous models and has previously been correlated to particle shape, with larger values produced by more irregular particles (Mueller et al., 2010). Pea hull fibre particles in the P-I samples are highly polydisperse and irregular which would yield a large exponent value. The  $\alpha$  value was interpreted by Mendoza to be affected by the particle deformation, as when particle deformability increases, the  $\alpha$  value decreases. A value of 2.2 was obtained for the P-I sample which is slightly higher than observed for star polymers (1.74-1.90), which would imply that the star polymers are more deformable. However, Leverrier and colleagues saw similar values for apple cells (2.10-2.16) and hypothesised that the  $\alpha$  value is also related to surface irregularities and sphericity (Leverrier et al., 2021). Leverrier and colleagues argue that lower surface irregularity and higher sphericity increase the value of  $\alpha$ . However, with our system, we achieve an even larger  $\alpha$  with non-spherical particles and high surface irregularities. The  $\beta$  value has been related to particle softness, with softer

**Table 4**

Models and obtained parameters used to fit the viscosity vs apparent volume fraction data for sample P-I.

Krieger-Dougherty	$\eta(\phi) = \eta_0 \left(1 - \frac{\phi}{\phi_{rcp}}\right)^{-k\phi_{rcp}}$ $\phi_{rcp}=0.637; k=3.9$
Mendoza	$\eta(\phi) = \eta_0 \left(1 - \frac{\phi}{1 - k\phi}\right)^{-[\eta]}$ $k = \frac{1 - \phi_c}{\phi_c}; \phi_c = \phi_{rcp} + \beta\phi^\alpha$ $\phi_{rcp}=0.637; [\eta]=10.4; \alpha=2.2; \beta=1.9$
Leverrier	$\eta(\phi) = \eta_0 \left(1 - \frac{\phi}{1 - k\phi}\right)^{-S}$ $k = \frac{1 - \phi_c}{\phi_c}; \phi_c = \phi_{rcp} + \frac{\phi_{max} - \phi_{rcp}}{1 + \exp[-\Lambda(\phi - \phi_i)]}$ $\phi_{rcp}=0.637; S=10.7; \phi_{max}=5.0; \phi_i=1.0; \Lambda=4.2$

Note: For eq. 8, 9 and 10,  $\eta(\phi)$  is the viscosity,  $\eta_0$  is the viscosity of the suspension liquid,  $\phi$  is the volume fraction,  $\phi_{rcp}$  is the volume fraction at random close packing.  $k$ ,  $[\eta]$ ,  $\beta$ ,  $\alpha$ ,  $S$ ,  $\phi_{max}$ ,  $\phi_i$  and  $\Lambda$  are coefficients.

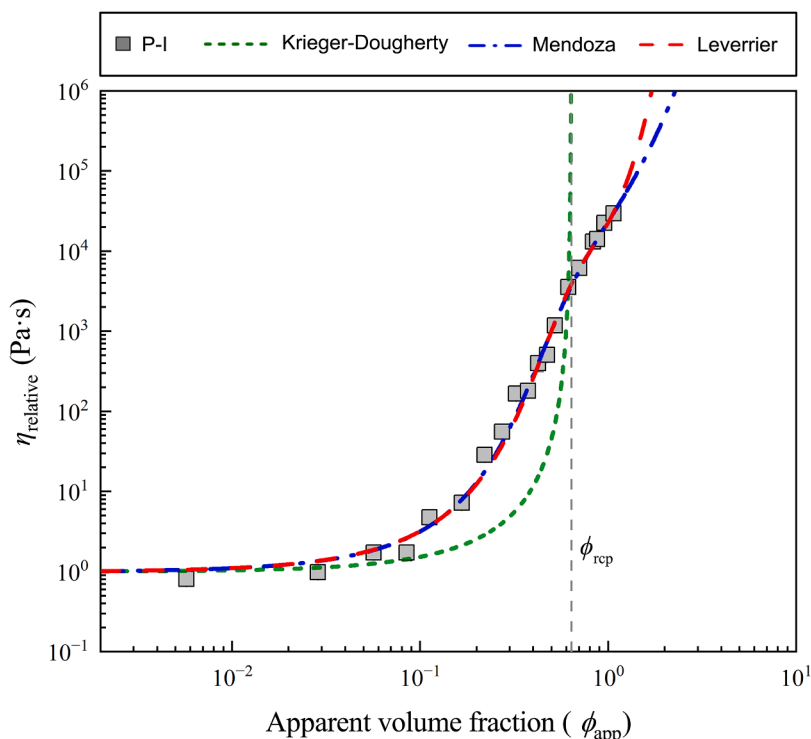


Fig. 7. Experimental data for reconstituted P-I sample suspension and theoretical modelling displaying the relative viscosity with the apparent volume fraction. Models and parameters can be found in Table 3. Symbols represent experimental data and lines relate to models.

particles producing a greater  $\beta$ . We obtained a value of 1.9, which is considerably larger than the  $\beta$  value obtained for star polymers (0.244-0.966) and apple cells (0.913-1.177), which in our case would indicate soft particles. The outer part of the pea hull fibre is expected to have a rigid structure (even if softened by the enzymatic hydrolysis) compared to the inner part of the fibre, whose structure would be softer.

Leverrier expanded on Mendoza's model and added a maximum packing fraction parameter ( $\phi_{\max}$ ) to limit the volume fraction to increase infinitely (Table 4) (Leverrier et al., 2021). The maximum packing fraction parameter is necessary as the soft particles will reach a maximal compression, which is dependent on the particles' nature. To calculate  $\phi_{\max}$ , a sigmoid law is used with additional parameters  $\phi_i$  and  $\Lambda$ , where  $\phi_i$  describes the point at which the particle concentration to particle compressibility is at a maximum and  $\Lambda$  is the slope after the inflection point. Lower values of  $\phi_{\max}$  and  $\phi_i$  (5.0 and 1.0, respectively) were obtained compared to apple cells (16.0 and 2.38). This shows that the P-I samples are deformable and able to fit into the available space at high concentrations but might be limited by the compressibility indicated by the  $\phi_i = 1$  value. The  $\Lambda$  is significantly larger than for apple cells (4.2 versus 1.87) further demonstrating that the  $\phi_{\max}$  will be reached at a lower volume fraction. Nonetheless, the high complexity of the P-I sample makes interpretation of the parameters non-trivial. A theoretical value derived from spheres of  $\phi_{\text{rcp}} = 0.635$  was used for all models, as its effect on the model outcome has been shown as negligible (Leverrier et al., 2021; Leverrier et al., 2017).

Overall, the model proposed by Mendoza and Leverrier fits the P-I experimental data through the entire concentration range. The Mendoza model was based on star polymers with a different number of arms. Leverrier and colleagues then introduced a maximum packing fraction parameter to the Mendoza model and showed that it also predicted the viscosity behaviour of apple cells as a function of volume fraction. The dispersions of pea hull fibre are of high complexity, as they contain large particles, with an irregular shape and surface and are largely poly-disperse. Nonetheless, the models proposed by Mendoza and Leverrier fitted the rheological behaviour of pea hull fibres well as a function of

volume fraction. Thus, the models can be used to predict the viscous behaviour of pea hull fibres over a wide concentration range.

#### 4. Conclusion

The results of this study demonstrated that the techno-functional properties of yellow pea hull fibres, especially rheological behaviour and water retention capacity (WRC) can be enhanced by a combination of mechanical shearing and enzymatic hydrolysis using pectate lyase. Among the treatment tested, the enzymatically treated sample (P) showed the most pronounced changes, including compositional changes, increased WRC, particle swelling and altered microstructure. While more soluble components are produced after shearing and enzymic treatment, flow sweep and oscillatory analysis demonstrated that the insoluble fraction was the main contributor to viscosity and viscoelasticity in all samples, with P-I sample displaying a marked increase in suspension properties.

Three distinct concentration regimes were identified for the P-I suspension: dilute, intermediate and concentrated. The behaviour across these regimes could be effectively modelled using soft particle rheological models originally proposed by Mendoza for star polymers and later expanded by Leverrier for apple puree. The models of Mendoza and Leverrier enable close prediction of suspension properties across several concentration regimes of the pea hull fibre. While the models were able to accurately predict viscosity behaviour, limitations remain in interpreting the parameters used in the models due to the high degree of complexity of the modified fibre structures.

Overall, these findings highlight the potential to transform the microstructure and techno-functional properties of pea processing side streams into high value functional ingredients for food applications. By tailoring hydration, swelling and predicting suspension properties, pea hull fibres can be more effectively as texturizing systems, fibre-enriched formulations, or plant-based food products, supporting both sustainability and functionality in food design.

## Ethical statement

This study did not involve any experiments on human participants or animals. All research was conducted using in vitro methods, computational modeling, or other non-animal, non-human approaches. Therefore, ethical approval was not required under institutional or national guidelines.

## CRedit authorship contribution statement

**Jakob Ytterberg:** Writing – original draft, Investigation, Formal analysis, Conceptualization. **Annika Krona:** Writing – review & editing, Supervision, Investigation. **Pamela Freire de Moura Pereira:** Writing – review & editing, Investigation. **Amparo Jimenez-Quero:** Writing – review & editing, Investigation. **Patricia Lopez-Sanchez:** Writing – review & editing, Supervision, Formal analysis, Conceptualization. **Anna Ström:** Writing – review & editing, Resources, Project administration, Funding acquisition, Formal analysis.

## Declaration of competing interest

The authors declare that they have no known competing financial interests or personal relationships that could have appeared to influence the work reported in this paper. None of the authors are an Editorial Board Member/Editor-in-Chief/Associate Editor/Guest Editor for Journal of Food Engineering and none has been involved in the editorial review or the decision to publish this article.

## Acknowledgements

The study was conducted under the PANSweden project, with financial support from the Swedish Research Council, FORMAS, grant no. 2020-02843. We thank Chalmers Materials Analysis Lab (CMAL) for access to the XRD instrument.

## Supplementary materials

Supplementary material associated with this article can be found, in the online version, at [doi:10.1016/j.fufo.2026.100945](https://doi.org/10.1016/j.fufo.2026.100945).

## Data availability

Data will be made available on request.

## References

- Adams, S., Frith, W.J., Stokes, J.R., 2004. Influence of particle modulus on the rheological properties of agar microgel suspensions. *J. Rheol.* 48 (6), 1195–1213. <https://doi.org/10.1122/1.1795193>.
- Auffret, A., Ralet, M.C., Guillon, F., Barry, J.L., Thibault, J.F., 1994. Effect of grinding and experimental conditions on the measurement of hydration properties of dietary fibres. *LWT - Food Sci. Technol.* 27 (2), 166–172. <https://doi.org/10.1006/fstl.1994.1033>.
- Bayod, E., Månsson, P., Innings, F., Bergenstahl, B., Tornberg, E., 2007. Low shear rheology of concentrated tomato products. Effect of particle size and time. *Food Biophys.* 2 (4), 146–157. <https://doi.org/10.1007/s11483-007-9039-2>.
- Boehm, M.W., Warren, F.J., Baier, S.K., Gidley, M.J., Stokes, J.R., 2019. A method for developing structure-rheology relationships in comminuted plant-based food and non-ideal soft particle suspensions. *Food Hydrocoll.* 96, 475–480. <https://doi.org/10.1016/j.foodhyd.2019.05.056>.
- Boukid, F., Rosell, C.M., Castellari, M., 2021. Pea protein ingredients: A mainstream ingredient to (re)formulate innovative foods and beverages. *Trends Food Sci. Technol.* 110, 729–742. <https://doi.org/10.1016/j.tifs.2021.02.040>.
- Broxterman, S.E., Schols, H.A., 2018. Interactions between pectin and cellulose in primary plant cell walls. *Carbohydr. Polym.* 192, 263–272. <https://doi.org/10.1016/j.carbpol.2018.03.070>.
- Day, L., Xu, M., Øiseth, S.K., Lundin, L., Hemar, Y., 2010. Dynamic rheological properties of plant cell-wall particle dispersions. *Colloids Surf. B: Biointerfaces* 81 (2), 461–467. <https://doi.org/10.1016/j.colsurfb.2010.07.041>.
- Einstein, A., 1906. Eine neue bestimmung der moleküldimensionen. *Ann. Phys.* 324 (2), 289–306. <https://doi.org/10.1002/andp.19063240204>.
- Farr, R., Groot, R., 2009. Close packing density of polydisperse hard spheres. *J. chem. phys.* 131, 244104. <https://doi.org/10.1063/1.3276799>.
- Farris, R.J., 1968. Prediction of the viscosity of multimodal suspensions from unimodal viscosity data. *Trans. Soc. Rheol.* 12 (2), 281–301. <https://doi.org/10.1122/1.549109>.
- Gutöhrlein, F., Morales-Medina, R., Boje, A.-L., Drusch, S., Schalow, S., 2020. Modulating the hydration properties of pea hull fibre by its composition as affected by mechanical processing and various extraction procedures. *Food Hydrocoll.* 107, 105958. <https://doi.org/10.1016/j.foodhyd.2020.105958>.
- Höfte, H., Peaucelle, A., Braybrook, S., 2012. Cell wall mechanics and growth control in plants: the role of pectins revisited. *Front. Plant Sci.* 3. <https://doi.org/10.3389/fpls.2012.00121>.
- Johansson, M., Karlsson, J., van den Berg, F.W.J., Ström, A., Ahrne, L., Sandström, C., Langton, M., 2024. Effect of cellulose-rich fibres on faba bean protein gels is determined by the gel microstructure. *Food Hydrocoll.* 156, 110295. <https://doi.org/10.1016/j.foodhyd.2024.110295>.
- Karlsson, J., Lopez-Sanchez, P., Marques, T.M., Hyötyläinen, T., Castro-Alves, V., Krona, A., Ström, A., 2024. Effect of heating of pea fibres on their swelling, rheological properties and in vitro colon fermentation. *Food Hydrocoll.* 147, 109306. <https://doi.org/10.1016/j.foodhyd.2023.109306>.
- Khelifi, H., Perrot, A., Lecompte, T., Rangaerd, D., Ausias, G., 2013. Prediction of extrusion load and liquid phase filtration during ram extrusion of high solid volume fraction pastes. *Powder Technol.* 249, 258–268. <https://doi.org/10.1016/j.powtec.2013.08.023>.
- Krieger, I.M., Dougherty, T.J., 1959. A mechanism for non-Newtonian flow in suspensions of rigid spheres. *Trans. Soc. Rheol.* 3 (1), 137–152.
- Kumari, T., Das, A.B., Deka, S.C., 2022. Effect of extrusion and enzyme modification on functional and structural properties of pea peel (*Pisum sativum* L.) insoluble dietary fibre and its effect on yogurt rheology. *Int. J. Food Sci. Technol.* 57 (10), 6668–6677. <https://doi.org/10.1111/ijfs.16012>.
- Kumari, T., Das, A.B., Deka, S.C., 2023. Effect of enzymatic modified pea peel dietary fibre on syneresis, texture, rheology and microstructural properties of yogurt. *Biomass Convers. Biorefinery.* <https://doi.org/10.1007/s13399-023-04933-z>.
- Leverrier, C., Almeida, G., Cuvelier, G., Menut, P., 2021. Modelling shear viscosity of soft plant cell suspensions. *Food Hydrocoll.* 118, 106776. <https://doi.org/10.1016/j.foodhyd.2021.106776>.
- Leverrier, C., Almeida, G., Espinosa-Munoz, L., Cuvelier, G., 2016. Influence of particle size and concentration on rheological behaviour of reconstituted apple purees. *Food Biophys.* 11 (3), 235–247. <https://doi.org/10.1007/s11483-016-9434-7>.
- Leverrier, C., Almeida, G., Menut, P., Cuvelier, G., 2017. Design of model apple cells suspensions: rheological properties and impact of the continuous phase. *Food Biophys.* 12 (3), 383–396. <https://doi.org/10.1007/s11483-017-9494-3>.
- Lopez-Sanchez, P., Chapara, V., Schumm, S., Farr, R., 2012. Shear elastic deformation and particle packing in plant cell dispersions. *Food Biophys.* 7 (1), 1–14. <https://doi.org/10.1007/s11483-011-9237-9>.
- Lopez-Sanchez, P., Farr, R., 2012. Power laws in the elasticity and yielding of plant particle suspensions. *Food Biophys.* 7 (1), 15–27. <https://doi.org/10.1007/s11483-011-9238-8>.
- Massironi, A., Freire De Moura Pereira, P., Verotta, L., Jiménez-Quero, A., Marzorati, S., 2024. Green strategies for the valorization of industrial medicinal residues of *Serenoa repens* small (saw palmetto) as source of bioactive compounds. *J. Environ. Manag.* 370, 122843. <https://doi.org/10.1016/j.jenvman.2024.122843>.
- Mendoza, C.I., 2013. Model for the shear viscosity of suspensions of star polymers and other soft particles. *Macromol. Chem. Phys.* 214 (5), 599–604. <https://doi.org/10.1002/macp.201200551>.
- Mewis, J., Wagner, N.J., 2009. Current trends in suspension rheology. *J. Non-Newton. Fluid Mech.* 157 (3), 147–150. <https://doi.org/10.1016/j.jnnfm.2008.11.004>.
- Mezzenga, R., Schurtenberger, P., Burbidge, A., Michel, M., 2005. Understanding foods as soft materials. *Nat. Mater.* 4 (10), 729–740. <https://doi.org/10.1038/nmat1496>.
- Morales-Medina, R., Dong, D., Schalow, S., Drusch, S., 2020. Impact of microfluidization on the microstructure and functional properties of pea hull fibre. *Food Hydrocoll.* 103, 105660. <https://doi.org/10.1016/j.foodhyd.2020.105660>.
- Morales-Medina, R., Manthei, A., Drusch, S., 2024. Enzymatic pre-treatment defines the water-binding and rheological properties of dynamic ultra-high-pressure homogenised pea hull suspensions. *Food Hydrocoll.* 157, 110454. <https://doi.org/10.1016/j.foodhyd.2024.110454>.
- Mueller, S., Llewellyn, E.W., Mader, H.M., 2010. The rheology of suspensions of solid particles. In: *Proceedings of the Royal Society A: Mathematical, Physical and Engineering Sciences*, 466, pp. 1201–1228. <https://doi.org/10.1098/rspa.2009.0445>.
- Poon, W.C., Weeks, E.R., Royall, C.P., 2012. On measuring colloidal volume fractions. *Soft Matter* 8 (1), 21–30. <https://doi.org/10.1039/C1SM06083J>.
- Quemada, D., 1977. Rheology of concentrated disperse systems and minimum energy dissipation principle. *Rheol. Acta* 16 (1), 82–94. <https://doi.org/10.1007/BF01516932>.
- Ralet, M.C., Della Valle, G., Thibault, J.F., 1993. Raw and extruded fibre from pea hulls. Part I: composition and physico-chemical properties. *Carbohydr. Polym.* 20 (1), 17–23. [https://doi.org/10.1016/0144-8617\(93\)90028-3](https://doi.org/10.1016/0144-8617(93)90028-3).
- Ramirez, C.S.V., Temelli, F., Saldaña, M.D.A., 2021. Production of pea hull soluble fiber-derived oligosaccharides using subcritical water with carboxylic acids. *J. Supercrit. Fluids* 178, 105349. <https://doi.org/10.1016/j.supflu.2021.105349>.
- Ratnayake, W.S., Naguleswaran, S., 2022. Utilizing side streams of pulse protein processing: A review. *Legume Sci.* 4 (1), e120. <https://doi.org/10.1002/leg3.120>.
- Rouquerol, J., Llewellyn, P., Rouquerol, F., 2007. Is the bet equation applicable to microporous adsorbents? In: *Llewellyn, P.L., Rodriguez-Reinoso, F., Rouquerol, J.,*

- Seaton, N. (Eds.), *Studies in Surface Science and Catalysis, Studies in Surface Science and Catalysis*, 160. Elsevier, pp. 49–56.
- Segal, L., Creely, J.J., Martin Jr, A.E., Conrad, C.M., 1959. An empirical method for estimating the degree of crystallinity of native cellulose using the X-ray diffractometer. *Text. Res. J.* 29 (10), 786–794. <https://doi.org/10.1177/004051755902901003>.
- Servais, C., Jones, R., Roberts, I., 2002. The influence of particle size distribution on the processing of food. *J. Food Eng.* 51 (3), 201–208. [https://doi.org/10.1016/S0260-8774\(01\)00056-5](https://doi.org/10.1016/S0260-8774(01)00056-5).
- Shewan, H.M., Stokes, J.R., 2015. Viscosity of soft spherical micro-hydrogel suspensions. *J. Colloid Interface Sci.* 442, 75–81. <https://doi.org/10.1016/j.jcis.2014.11.064>.
- Sluiter, A., Hames, B., Ruiz, R., Scarlata, C., Sluiter, J., Templeton, D., Crocker, D., 2008. Determination of structural carbohydrates and lignin in biomass. *Laboratory Analytical Procedure (LAP)*. Retrieved from.
- Tosh, S.M., Yada, S., 2010. Dietary fibres in pulse seeds and fractions: characterization, functional attributes, and applications. *Food Res. Int.* 43 (2), 450–460. <https://doi.org/10.1016/j.foodres.2009.09.005>.
- Uluşık, S., Seymour, G.B., 2020. Pectate lyases: their role in plants and importance in fruit ripening. *Food Chem.* 309, 125559. <https://doi.org/10.1016/j.foodchem.2019.125559>.
- Wu, P., Yang, S., Zhan, Z., Zhang, G., 2020. Origins and features of pectate lyases and their applications in industry. *Appl. Microbiol. Biotechnol.* 104 (17), 7247–7260. <https://doi.org/10.1007/s00253-020-10769-8>.